J Exp Biol Advance Online Articles. First posted online on 20 July 2017 as doi:10.1242/jeb.162511
Access the most recent version at http://jeb.biologists.org/lookup/doi/10.1242/jeb.162511

Flowtrace: simple visualization of coherent structures in biological fluid flows

William Gilpin[1], Vivek N. Prakash[2], Manu Prakash[2*]

[1]Department of Applied Physics, [2]Department of Bioengineering,

Stanford University, Stanford, CA

*To whom correspondence should be addressed; E-mail: manup@stanford.edu

Key words: visualization, fluid dynamics, streamlines

© 2017. Published by The Company of Biologists Ltd.

Journal of Experimental Biology • Advance article

Abstract

We present a simple, intuitive algorithm for visualizing time-varying flow fields that can reveal complex flow structures with minimal user intervention. We apply this technique to a variety of biological systems, including the swimming currents of invertebrates and the collective motion of swarms of insects. We compare our results to more experimentally-difficult and mathematically-sophisticated techniques for identifying patterns in fluid flows, and suggest that our tool represents an essential "middle ground" allowing experimentalists to easily determine whether a system exhibits interesting flow patterns and coherent structures without resorting to more intensive techniques. In addition to being informative, the visualizations generated by our tool are often striking and elegant, illustrating coherent structures directly from videos without the need for computational overlays. Our tool is available as fully-documented open-source code available for MATLAB, Python, or ImageJ at www.flowtrace.org.

Journal of Experimental Biology • Advance article

1 Introduction

Flow visualization is an essential technique for studying biological processes arising in many diverse areas, including ecology,[1] biomechanics,[2] and molecular biology.[3, 4] Observations of the trajectories of many tracer particles—whether fluorescent beads, microbubbles, vesicles inside a moving cell, or flocking bacteria—can reveal rich information about the way that biological motion such as molecular transport, ciliary flows, or active force generation is coordinated over many length and timescales.[5–8] Additionally, flow visualization aids in characterization and secondary validation of many standard techniques, such as microfluidics and flow cytometry.[9, 10]

The simplest qualitative flow visualization techniques involve observations of the motion of passive scalars, like dyes or smoke, as they are advected by the flow. These experiments have the benefit of being relatively straightforward to perform, and can often yield immediate insight into the global structure and mixing properties of a flow.[11] However, at length and time scales dominated by diffusive effects, or in flows characterized by large separations in the timescales of different processes, the results of such studies can be difficult to interpret.[12, 13] As a result, in many contexts quantitative flow characterization techniques based on the motion of tracer particles are preferable.[14–16]

However, standard quantitative flow visualization techniques—particle tracking and particle image velocimetry (PIV)—are sufficiently difficult to implement and optimize that these rigorous fluid dynamical visualization techniques remain prohibitive in many experimental contexts.[13] While PIV and related techniques have been widely-applied and optimized for certain biological systems, such as the study of fish swimming[17] or bloodflow mechanics,[8] in less-established contexts these techniques require specialized modifications of apparatuses such as laser light sheets to be constructed.[4, 18] As a result, system-specific techniques are often necessary,[19] particularly when particle motion is only partially visible in the data, such as from image streaks[9] or out-of-focus drift due to limited depth of field.[20] This issue is even more prominent for flows in non-traditional media, such as in the collective motion of flocks

Journal of Experimental Biology • Advance article

and herds.[21–23]

Nonetheless, many standard concepts in fluid mechanics—such as vortices, jets, and turbulence—are widely-known to researchers throughout the sciences, who may recognize the likely presence of these features in their data even without the need for quantitative flow characterization tools.[24, 25] This suggests that simpler flow visualization tools are necessary for systems in which dye-based qualitative techniques are unavailable, but quantitative tracer-particle studies are unnecessary.

Here, we describe Flowtrace, an algorithm and associated open-source tool that can assist in identifying characteristic flow structures in experimental videos. This primarily qualitative technique is sufficiently straightforward and intuitive to be used either as a primary analysis tool for presence/absence studies, or to motivate the use of more complicated flow quantification methods. The technique is based purely on image processing of the input data, rather than numerical reconstruction of scalar fields like vorticity, allowing it to be used as a straightforward "first pass" characterization technique for biological systems where traditional techniques are either unnecessary to support qualitative observations, or prohibitively difficult due to the length- and time-scales involved. While Flowtrace is a straightforward algorithm, to our knowledge it has not been reported or widely adopted in the literature—and, importantly, we find that it has surprising utility for studying flow patterns in a wide range of biological data sets.

2 Materials and Methods

2.1 Algorithm

The algorithm generalizes a common technique for generating long-exposure photographs from videos, in which the maximum (or minimum) intensity projection of a time series of images is taken in order to generate pathlines for bright objects moving against a dark background—resulting in "motion streaks" across the image.[5] This technique has previously

Journal of Experimental Biology • Advance article

been used to create star trails, a popular astronomical visualization generated by taking the maximum intensity projection of a stabilized video of the night sky.[26]

Flowtrace primarily extends this technique by using a single long experimental video, and then iteratively taking the maximum intensity projection of small groups of successive video frames in order to generate sequential images showing pathlines at different times. The resulting time series of pathline images reveals how the shapes of the pathlines change over time. For example, in a 100 frame raw experimental video, a Flowtrace video with 30-frame traces consists of the maximum intensity projection of frames 1-31, 2-32, 3-33, etc, and so forth. The sequence ends when frames 70-100 are projected, resulting in a 70 frame video. In addition to this basic operation, various other operations can be combined with the maximum intensity projection operator in order to yield improved results. The process is illustrated graphically in Figure 1C.

Symbolically, let each frame of the movie be a vector of pixel values and locations, $v_{ij}[t]$, where $t = 1, 2, ..., N$ represents the index of a frame in a video consisting of N frames, and i and j denote the coordinates of a pixel in the image. Suppose that the tracer particles are brightly-colored objects moving against a dark background. In this case, a series of maximum-intensity projections, $\mathbf{p}[t]$, may be defined in terms of a forward convolution operator,

$$\mathbf{p}[t] = (\mathbf{P} * \mathbf{v})[t]$$

$$\text{where} \quad (P_{ij} * v_{ij})[t] \equiv \max_{t' \in \{1,2,...,M\}} v_{ij}^{t+t'}$$

where $M < N$ is some subset of the frames in the video. As the time index t "slides" forward across successive indices $1, 2, 3, ...$, the maximum intensity projection is taken across successive runs of M frames that each differ by two images (the first and the last). This results in a set of maximum intensity projections, $p_{ij}^t, t = 1, 2, ..., N - M$, that constitute a new video generated from the original data set. Importantly, the number of frames in the

Journal of Experimental Biology • Advance article

generated video ($N - M$) is almost equal to the number of frames in the original video (N). In this paper, we refer to each subsequence of M images as a *substack*, and the sequence of positions taken by a single particle moving across M frames as a *pathline*. The parameter M, the timescale over which particle pathlines are visualized in each frame, represents the only parameter that the user must specify in order to use the tool. For a time series of images taken with a fixed time spacing Δt (equivalent to $1/(\text{frame rate})$), the total pathline projection time is defined as $\tau \equiv M\,\Delta t$.

During convolution, the projection operator $\mathbf{P}$ "slides" across the entire sequence of frames, operating on the video in overlapping sets of M frames. This operator can be composed with other pre-processing operations in order to achieve different effects; in the code described below, other operations defined include median subtraction (to remove slowly-moving objects), color inversion (for dark objects moving against a lighter background), differential weighing (coloring or darkening each frame in the M frame sequence a different amount, in order to show a gradient across the pathlines indicating time), and pairwise differencing (to isolate objects that move faster than 1 px/frame). Each of these operations symbolically represents composition before convolution, such that the final image series is $((\mathbf{P} \circ \mathbf{G}) * \mathbf{v})[t]$, where $\mathbf{G}$ is the pre-processing operation.

2.2 Software package and options

The algorithm is implemented as an open-source package for MATLAB, Python, or ImageJ at www.flowtrace.org. Full tutorials and sample image sets are provided there. Table 1 summarizes the primary user-specified arguments and options available for the code; optional arguments are passed as a *struct* object in MATLAB, as keyword arguments in Python, and as checkboxes in a GUI for ImageJ.

The primary options for the software involve removal of background drift and crossing pathlines, which complicate interpretation of the videos. Oftentimes a dataset features two well-separated velocity scales: one for advected tracer particles and one for background drift,

Journal of Experimental Biology • Advance article

bulk flow, etc. In these cases Flowtrace performs best when the projection time τ is sufficient for fast particles to travel far within the field of view, while relatively slow objects move very little. This is true for the pathlines shown for the two feeding current-generating organisms shown in Figure 1, for which τ is long compared to the mean transit time of tracer particles, but short compared to the gradual motion of each organism's body. As a result, features of each organism's anatomy remain sharp in the image. However, in many cases particle advection timescales are not well separated from background motion (resulting in motion blur for slowly-moving objects) or stationary objects and obstacles in the image obscure the pathlines. In these cases, it is useful to apply a background subtraction operation to each substack before performing the projection (the "take_difference" option in the software). For objects moving slowly relative to the tracer particles, but fast enough to exhibit noticeable motion blur, the most aggressive background-subtraction option available in the software takes the pairwise differences among all consecutive images before applying the projection. However, moving tracer particles that move less than a pixel between successive frames will also vanish. Alternate background subtraction options in Flowtrace include subtracting either the median or the first image from stack before projection ("take_median" or "take_first", respectively). Occasionally it is convenient to highlight the direction of time in the pathlines, particularly when still frames from the output time series are used for analysis. In this case, directionality can be indicated by applying a color gradient across time ("color_series"), or by applying a linear intensity gradient ("fade_tails").

2.3 Software availability

The source code for Flowtrace is available for Fiji, ImageJ, Python 2, Python 3, and MATLAB. The full code base, as well as screenshots, tutorials, and installation instructions, may be accessed at `http://www.flowtrace.org`. Table 1 summarizes the primary user-specified arguments and options available for the code; optional arguments are passed as a *struct* object in MATLAB, as keyword arguments in Python, and as checkboxes in a GUI for

Table 1 Options and parameters for Flowtrace. Full documentation for individual versions of Flowtrace for ImageJ, Python, and MATLAB can be found at www.flowtrace.org

Required Argument (type)	Description
frames_to_merge (integer)	The number of input frames to combine per output frame
image_dir (string)	The location to save output files
Optional Argument (type)	Description (default)
invert_color (boolean)	For images comprising dark objects moving against a light background (false)
subtract_median (boolean)	Subtract the median of the substack from the substack before projection (false)
take_difference (boolean)	Take the pairwise differences of images before projection (false)
subtract_first (boolean)	Subtract the first image of each substack from the substack before projection (false)
add_first (boolean)	Add the first image of each substack to each projected image (false)
color_series (boolean)	Apply a color gradient across pathlines (false)
frames_to_skip (integer)	Number of alternate frames to omit from each projection (0)
use_parallel (boolean; Python only)	Use multithreading across cores (false)
max_cores (integer; Python only)	The maximum number of threads to use when running in parallel (4)
fade_tails (boolean; MATLAB only)	Apply an intensity gradient across pathlines (false)

ImageJ.

The individual GitHub repositories and version histories for the three implementations are open for pull requests and forks on GitHub at `https://github.com/williamgilpin/flowtrace_imagej`, `https://github.com/williamgilpin/flowtrace_python`, and `https://github.com/williamgilpin/flowtrace_matlab`. A gallery of videos generated using the technique is available at `http://www.flowtrace.org/flowtrace_docs/gallery.html`

2.4 Experimental Methods

For bead studies, organisms were placed in a droplet of water (or an appropriate saline buffer) on a glass slide. A $1:100$ dilution mixture of 6 μm polystyrene beads was placed into the droplet and gently mixed using a pipette tip. A 22 coverslip was prepared by dragging each of its corners through modeling clay, resulting in "feet" of $500-600$ μm height. The coverslip was then placed on the slide feet-down, such that the organism was confined between the slide and the cover slip. Images were captured using an ORCA C11440 CCD, (for color panels, a Canon EOS T3i DSLR or an Apple iPhone 5s was used). Videos were split into single frames using Fiji, and the resulting time series of images were processed using the Flowtrace software. The three implementations (Fiji/ImageJ, MATLAB, and Python 2 and 3) yield the same results. Methods specific to individual datasets are described below:

Supplementary Video 1: An eight-week old starfish larvae modulates its swimming currents in order to increase the vorticity it generates, and thus its feeding rate. This video is taken from Gilpin et al.,[27] which discusses this phenomenon in more detail. This video was captured at 4x magnification and 20 fps on an inverted Nikon microscope with dark field illumination; the water contains 6 μm beads. The projection time is $\tau = 3$ s, and the video is shown at 8x true speed.

Supplementary Video 2: *Stentor sp.* generates a large dipolar feeding current using its primary ciliary band. This current is periodically disrupted when the organism rotates its stalk to invert the position of the ciliary stripes. A full 180 degree rotation of the organism

Journal of Experimental Biology • Advance article

(and its associated feeding currents) is shown in the video. Images were captured at 30x magnification and 20 fps on an inverted Nikon microscope; the water contains 6 μm beads as well as algae and other detritus advected by the feeding current. In Flowtrace, "subtract median" was used to remove background objects. The projection time was $\tau = 3$ s, and the video is shown at 8x true speed.

Supplementary Video 3: A hyperbolic stagnation point represents a transport barrier for the cerebrospinal fluid in a mouse brain ventricle. Original video taken by Faubel et al[28] using 1 μm fluorescent spheres as tracer particles. In Flowtrace, "subtract median" was used to remove background objects and gradual variations in overall intensity across the image. The projection time was $\tau = 0.67$ s, and the video is shown at 1x true speed.

Supplementary Video 4: A sea anemone pumps seawater into its body cavity, creating a short-lived jet that entrains particles. The animal was suspended in filtered sea water containing 6 μm beads. Videos were taken at 1 fps on an ORCA C11440 CCD and Nikon microscope with 1x magnification. In Flowtrace, "subtract median" was used to remove background objects, and the final projected movies were color-inverted to ease visualization. The projection time was $\tau = 240$ s, and the video is shown at 48x true speed

Supplementary Video 5: A two-day old veliger larva of a moon snail generating a steady dipolar feeding current, punctuated by brief interruptions. The animal was suspended in filtered sea water with red 6 μm beads. Images were taken at 30 fps on a Canon EOS T3i DSLR and Nikon microscope with 10x magnification. In Flowtrace, "subtract median" was used to remove background objects. The projection time was $\tau = 2$ s, and the video is shown at 8x true speed.

Supplementary Video 6: A swarm of flying midges gradually tightens in shape. Original video taken at 170 fps by Attanasi et al.[29] In Flowtrace, "subtract median" and "color series" were enabled in order to remove background objects and color-code the resulting images by time. The projection time was $\tau = 333$ ms, and the video is shown at 1/6x true speed.

Journal of Experimental Biology • Advance article

Supplementary Video 7: A school of 70 fish undergoes a spontaneous transition from a "milling" to "swarming" behavioral state. Original video taken by Tunstrøm et al.[30] In Flowtrace, "subtract median" and "fade tails" were enabled in order to remove background objects and intensity-code the resulting images by time. The projection time was $\tau = 5.33$ s.

Supplementary Video 8: The feeding current of the sessile, predatory protozoan *Stentor* in a sample of pond water. The large dipolar entrainment flow field generated by the organism captures some particles, but some smaller algae and other swimming organisms in the water appear to easily escape the vortices. This video was captured at 4x magnification and 20 fps on an inverted Nikon microscope with dark field illumination. The projection time was $\tau = 3$ s, and the video is shown at 8x true speed

2.5 Comparison and validation with other techniques

Quantitative flow visualization involves using image analysis techniques to take discrete integral transforms of a data set, either for the sake of performing convolution in order to extract a velocity field (PIV) or in order to establish unique identities of objects (as in PTV). In these methods, a underlying model of the flow is assumed by the technique, and coherent structures may be visualized either by numerically integrating trajectories, or by defining a spatially-resolved scalar field (such as the strain or vorticity) and plotting contours. The techniques compared here (PIV and PTV) are subject to the basic drawbacks: they can be computationally demanding, and require the experimental data set to have certain properties (such as narrow depth of field or high tracer particle density) in order to be well posed.

Figure 2 compares pathlines generated by Flowtrace to several common methods of detecting coherent structures based on PIV data. A video on larval starfish swimming published in a previous study is used as a test dataset.[27] In the referenced video, Flowtrace shows a stable arrangement of slowly-varying vortices around the periphery of a starfish larva held stationary (see Figure 1 and Supplementary Video 1 of the referenced paper).[27]

Journal of Experimental Biology • Advance article

2.5.1 Vorticity

One simple type of flow visualization involves isocontours of vorticity and other scalar fields derived from PIV. For the analysis in Figure 2C, the vorticity correctly localizes to regions of the flow corresponding to steady vortices, and the color and intensity of the shaded regions matches the apparent local rotation directions and intensity based on the length and direction of the pathlines. Thus, for persistent vortex structures the vorticity field and the pathlines agree.

However, it is apparent in the Figure that, as a metric based on taking the spatial derivative of experimental data, the vorticity has large spatial noise, despite the velocity field having been averaged across time and space to reduce correlation errors in the PIV.[31] Whether noise comes from the precision of the PIV measurement, or true fluctuations in the amplitude of the velocity field across space, this noise complicates interpretation of basic qualitative questions, such as the exact locations and relative sizes of the vortical regions. Because calculation of vorticity relies upon some underlying assumptions regarding the flow in the form of the relative mesh size and spatial and temporal averaging applied to the PIV data set, vorticity and similar finite-difference metrics can misplace the center point or relative scale of vortex structures.[32] Thus, for qualitative observations in slowly-varying flows, Flowtrace may be preferable for identifying coherent structures like vortices.

However, a case where vorticity plots and Flowtrace yield different qualitative visualizations arises in quickly time-varying flows, in which vorticity may be short-lived enough that particles do not have sufficient time to circumscribe vortices. For example, studies of the swimming flagellate *Chlamydomonas* report closed streamlines both in the instantaneous velocity field[33] and in the velocity field averaged across multiple flagellar beat cycles.[34] However, due to the time-varying structure of this field during the beat, areas of high vorticity move between the fore and aft of the organism during the swimming stroke,[33] and so pathlines generated by Flowtrace would show non-closed and potentially overlapping paths. Thus, plotting a scalar field from PIV (like vorticity) may be preferable when the timescales

Journal of Experimental Biology • Advance article

of particle advection within the field of view is comparable to the timescale of flow variation. A similar argument would apply to other common scalars computed as the finite differences of PIV data, such as the strain and shear,[35, 36] as well as more sophisticated techniques based on computing Eulerian quantities like the local acceleration.[37, 38]

2.5.2 Finite-time Lyapunov Exponents

More sophisticated tools for the identification of structures in time-varying flows are based on the detection of "Lagrangian Coherent Structures" (LCS), which are bounded regions of a flow with dynamics that are qualitatively distinct from the rest of the flow.

For example, at high Reynolds number, vorticity is conserved and remains localized, causing patches of vorticity that remain intact as they are advected by the flow. In this case, the patches of vorticity essentially act as tracers, even in turbulent conditions.[39] Vortices at high Reynolds numbers thus represent examples of "attracting LCS," which are bounded regions that tend to pull trajectories of neighboring particles towards themselves, and in some cases are mathematically equivalent to the "islands of stability" observed in the solutions of classical dynamical systems exhibiting chaos.[40] Based on this analogy, LCS can be identified using the finite-time Lyapunov exponent (FTLE), a computationally-efficient approximation of the classical Lyapunov exponent, which measures the tendency of trajectories originating from a given location to diverge or converge over time.[41] The derivation and properties of the FTLE are discussed in detail in many recent reviews;[42, 43] for our purposes it is a scalar-field defined across space that can be used to identify regions in a flow that attract or repel trajectories.

While LCS are fundamentally a property of the underlying velocity field present in a system, they can often be visualized through the manner in which they advect passive tracers—hence why coherent flow structures such as smoke rings or whirlpools are easily visualized.[42] Thus the FTLE field should detect key features visible in the pathline output of Flowtrace, such as vortices and stagnation points.

Figure 2 (panels B and D) shows the result of computing the FTLE field for the starfish dataset. First, PIV was applied to the original video in order to generate an estimate of the velocity field as a function of time at various points on a fixed spatial mesh.[44] Then the FTLE field was generated by interpolating this field and numerically integrating trajectories originating from various points in the image, using a tool developed by the Dabiri group.[45] The FTLE field was then smoothed with a median filter with a width equal to the size of the lattice on which the PIV field was calculated, in order to remove artifacts in the field arising from discretization of space. The resulting scalar field contains both positive (red) and negative (blue) values, and in the figure it is overlaid on the first frame of a Flowtrace video for the same data set.

Figure 2 shows FTLE fields for both forwards (panel D) and backwards (panel B) integration schemes, which respectively detect repelling and attracting LCS in the flow field. In both cases, the locations of the highest absolute intensity localize to the regions between two vortices, with streamlines that diverge in time generating regions with high positive FTLE values (red regions in the forward time plot) and regions with converging streamlines having large negative FTLE values (red regions in the backward time plot). The "zero FTLE" contours clearly run orthogonally to the pathlines shown by Flowtrace, as would be expected for a quasi-steady flow. The peaks and minima of the FTLE field roughly correspond to the locations of stagnation points along the boundary of the animal, with stagnation points that result in jet-like ejections of water from the surface having large positive FTLE regions, and stagnation points that pull water into the surface having large negative FTLE regions. The FTLE field and the pathlines shown by Flowtrace thus yield good agreement.

However, the FTLE field by itself is not straightforward to interpret—isocontours of the computed field do not necessarily indicate separatrices in the flow field. This is due, in part, to the lack of guaranteed coincidence of FTLE ridges with true material lines (transport barriers) in finite-time simulations.[46] In general, there is some ambiguity regarding the optimal algorithm for the definition of "ridges" in an FTLE field.[42, 47] However, for a quasi-

Journal of Experimental Biology • Advance article

static flow field such as the one shown in the Figure, Flowtrace is able to clearly delineate pathlines belong to different vortex regions, because the pathlines show true transport in the system.

However, recently more sophisticated topology-based techniques based on the adjacency matrix associated with neighboring trajectories (instead of changes in the Euclidean distance) allow coherent structures to be determined from sparser data sets (such as those generated by particle tracking experiments).[48] However, identification of structures with high spatial resolution still requires interpolation of the velocity field and subsequent integration of trajectories, leading it to be susceptible to the same limitations as the above.

Finally, the quality of the FTLE field and the associated ridges and minima that signal the presence of LCS is highly dependent on the quality and resolution of the PIV data from which the field is generated. Thus LCS detection does not solve the original issue that motivates the use of Flowtrace, that of creating a simple and straightforward qualitative visualization technique that requires comparatively less experimental optimization. However, it does confirm that, at least for quasi-static cases, Flowtrace is capable of identifying transport barriers in a flow, which are essential for gaining qualitative understanding.

3 Results and Discussion

Application of Flowtrace to a variety of biological systems provides surprising insight into the complicated dynamics of unsteady flows. By varying the projection time interval, τ (and thus the pathline lengths), biological phenomena may be investigated over a wide range of length and time scales. Detailed methods for each of the experiments and Supplementary Videos are discussed in the Materials and Methods.

Figure 1A shows three representative frames from a Flowtrace movie of a starfish larva (*Patiria miniata*), which in previous work we have shown creates dynamic vortex arrays around its body as it continuously adjusts its feeding currents.[27] The full Flowtrace movie

Journal of Experimental Biology • Advance article

from which the figure panel is generated shows the animal smoothly alternating between distinct swimming and feeding vortex patterns, indicating how these dynamic flow patterns represent distinct behaviors controlled by animal (Supplementary Video 1; discussed further in the referenced paper).[27] Figure 1B shows similar ciliary flows generated during stationary filter feeding by the protozoan *Stentor sp.* (size $\sim 50\mu m$), which generates a toroidal current that draws small prey towards its stalk. The videos and images ($\tau = 3$ s) capture the helical motion of algae particles as the organism slowly rotates its stalk (Supplementary Video S2), and a larger field of view shows the effect of the feeding current on microorganisms swimming nearby (Supplementary Video S8).

Flowtrace can be applied to any standard experimental data in which tracer particles (such as fluorescent beads) travel for an extended period in the imaging plane. Application of the tool to data from a recent study of ciliary currents generated in a mouse brain reveals the presence of a prominent hyperbolic stagnation point associated with a transport barrier in the cerebrospinal fluid, an observation identified using a full particle tracking in the original study[28] (Figure 3A, Supplementary Video S3). A similar technique allows identification of coherent flow structures formed by the sea anemone *Aiptasia pallida* ($\sim$ 1 mm): an inverted-color Flowtrace video ($\tau = 4$ min) shows the breakup of a water jet as the animal peristaltically pumps water into its body cavity (Figure 3B, Supplementary Video S4). In a color DSLR video of the larva of the moon snail *Crepidula fornicata* ($\sim$ 1 mm), Flowtrace creates a color video by projecting each channel separately, generating a true color video of the formation of the dipolar flow field created by the swimming animal (Figure 3C, Supplementary Video S5).

In addition to passive fluid tracer particles, Flowtrace can be applied to active particles and ecological data. For these datasets, applying a color or brightness gradient along the pathlines proves beneficial when many pathlines overlap due to particles appearing in the same location at different times. Figure 4 shows an application of two such cases taken from the collective motion literature.[29, 30] In a swarm of flying midges (*Dasyhelea flavifrons*, flock

Journal of Experimental Biology • Advance article

∼1 m wide), Flowtrace with color gradient across time allows rapid tightening of the flock to be visualized (Figure 4A, Supplementary Video S6, raw data taken from the referenced paper).[29] Similarly, in a video of 70 freely-swimming minnows (*Notemigonus crysoleucas*), Flowtrace can be used to identify changes in the schooling behavior: the school undergoes a transition from a visibly-rotary "milling" state, to a directionally-aligned collective state, to a disordered "swarm" state (Figure 4B, Supplementary Video S7, raw data taken from the referenced paper).[30] Relative to the raw video, the Flowtrace video makes it easier to visualize the onset of these transitions, which arise when a subset of individuals spontaneously polarizes and travels in a single direction.

The simple sliding projection technique used by Flowtrace appears to be largely-unknown in the biological sciences and fluid dynamics literature, despite the ease with which it can be implemented. Flowtrace can reproduce the core qualitative conclusions of several studies, including our recent study on larval starfish swimming,[27] in which the key observation of distinct feeding and swimming vortex arrays generated by the animals is readily seen in Flowtrace videos but difficult to discern using particle image velocimetry, the standard method of analyzing such data.[4] The algorithm works particularly well for studies of organismal feeding currents, in which there is a wide separation between the timescales of advection and behavior-driven flow variation—such that tracer particles have sufficient time to map out the structure of the flow field before the field undergoes further variation. Moreover, feeding phenomena typically involve small length scales and long timescales, for which traditional dye advection visualization techniques would fail due to rapid diffusive mixing.

Flowtrace has been compared to other techniques for identifying structures in fluid flows, and it can qualitatively reproduce the results of more-sophisticated dynamical analysis using either vorticity contours or finite-time Lyapunov exponents.[42, 45] The tool is available in efficient, multithreaded implementations for Fiji/ImageJ, Python 2 and 3, and MATLAB. A broad community—from microscopists to ecologists to fluid physicists—may use and even further improve Flowtrace, and so the full source code and documentation is available at

Journal of Experimental Biology • Advance article

http://www.flowtrace.org or for pull requests on GitHub.

4 Acknowledgements

The authors thank L. Y. Esherick and J. R. Pringle for providing anemones, and D. N. Clarke and C. J. Lowe for providing microscopy equipment and moon snails.

5 Competing Interests

The authors declare no competing interests.

6 Funding

This work was supported by a National Science Foundation Graduate Research Fellowship (DGE-114747) and a National Geographic Society Young Explorers Grant (to W. G.); and an ARO MURI Grant W911NF-15-1-0358 and National Science Foundation CAREER Award (to M. P.).

7 Data Availability

The full video datasets corresponding to each figure are available online:

Supplementary Video 1: https://vimeo.com/190107827

Supplementary Video 2: https://vimeo.com/144085848

Supplementary Video 3: https://vimeo.com/203738517

Supplementary Video 4: https://vimeo.com/144105031

Supplementary Video 5: https://vimeo.com/144085960

Supplementary Video 6: https://vimeo.com/144072652

Supplementary Video 7: https://vimeo.com/190801053

Journal of Experimental Biology • Advance article

References

[1] Rohr, J., Hyman, M., Fallon, S. & Latz, M. I. Bioluminescence flow visualization in the ocean: an initial strategy based on laboratory experiments. *Deep Sea Research Part I: Oceanographic Research Papers* **49**, 2009–2033 (2002).

[2] Bartol, I. K., Krueger, P. S., Jastrebsky, R. A., Williams, S. & Thompson, J. T. Volumetric flow imaging reveals the importance of vortex ring formation in squid swimming tail-first and arms-first. *Journal of Experimental Biology* **219**, 392–403 (2016).

[3] Boot, M. J. *et al.* In vitro whole-organ imaging: 4d quantification of growing mouse limb buds. *Nature Methods* **5**, 609–612 (2008).

[4] Lindken, R., Rossi, M., Große, S. & Westerweel, J. Micro-particle image velocimetry (μpiv): recent developments, applications, and guidelines. *Lab on a Chip* **9**, 2551–2567 (2009).

[5] Shapiro, O. H. *et al.* Vortical ciliary flows actively enhance mass transport in reef corals. *Proceedings of the National Academy of Sciences* **111**, 13391–13396 (2014).

[6] Han, S. J., Oak, Y., Groisman, A. & Danuser, G. Traction microscopy to identify force modulation in subresolution adhesions. *Nature Methods* **12**, 653–656 (2015).

[7] Deforet, M. *et al.* Automated velocity mapping of migrating cell populations (AVeMap). *Nature Methods* **9**, 1081–1083 (2012).

[8] Bharadvaj, B., Mabon, R. & Giddens, D. Steady flow in a model of the human carotid bifurcation. part i?flow visualization. *Journal of biomechanics* **15**, 349–362 (1982).

[9] Santiago, J. G., Wereley, S. T., Meinhart, C. D., Beebe, D. & Adrian, R. J. A particle image velocimetry system for microfluidics. *Experiments in fluids* **25**, 316–319 (1998).

[10] Eyal, S., Quake, S. R. *et al.* Velocity-independent microfluidic flow cytometry. *Electrophoresis* **23**, 2653–2657 (2002).

Journal of Experimental Biology • Advance article

[11] Merzkirch, W. *Flow visualization* (Elsevier, 2012).

[12] Miyake, R., Lammerink, T. S., Elwenspoek, M. & Fluitman, J. H. Micro mixer with fast diffusion. In *Micro Electro Mechanical Systems, 1993, MEMS'93, Proceedings An Investigation of Micro Structures, Sensors, Actuators, Machines and Systems. IEEE.*, 248–253 (IEEE, 1993).

[13] Miles and, R. B. & Lempert, W. R. Quantitative flow visualization in unseeded flows. *Annual review of fluid mechanics* **29**, 285–326 (1997).

[14] Bayraktar, T. & Pidugu, S. B. Characterization of liquid flows in microfluidic systems. *International Journal of Heat and Mass Transfer* **49**, 815–824 (2006).

[15] Mercado, J. M. *et al.* Lagrangian statistics of light particles in turbulence. *Physics of Fluids (1994-present)* **24**, 055106 (2012).

[16] Kertzscher, U., Berthe, A., Goubergrits, L. & Affeld, K. Particle image velocimetry of a flow at a vaulted wall. *Proceedings of the Institution of Mechanical Engineers, Part H: Journal of Engineering in Medicine* **222**, 465–473 (2008).

[17] Stamhuis, E. & Videler, J. Quantitative flow analysis around aquatic animals using laser sheet particle image velocimetry. *Journal of Experimental Biology* **198**, 283–294 (1995).

[18] Adrian, R. J. & Westerweel, J. *Particle image velocimetry*. 30 (Cambridge University Press, 2011).

[19] Stamhuis, E., Videler, J., van Duren, L. & Müller, U. Applying digital particle image velocimetry to animal-generated flows: Traps, hurdles and cures in mapping steady and unsteady flows in re regimes between 10–2 and 105. *Experiments in Fluids* **33**, 801–813 (2002).

Journal of Experimental Biology • Advance article

[20] Olsen, M. & Adrian, R. Out-of-focus effects on particle image visibility and correlation in microscopic particle image velocimetry. *Experiments in fluids* **29**, S166–S174 (2000).

[21] Garcimartín, A. *et al.* Flow and clogging of a sheep herd passing through a bottleneck. *Physical Review E* **91**, 022808 (2015).

[22] Attanasi, A. *et al.* Information transfer and behavioural inertia in starling flocks. *Nature physics* **10**, 691–696 (2014).

[23] Vicsek, T. & Zafeiris, A. Collective motion. *Physics Reports* **517**, 71–140 (2012).

[24] Rau, K. R., Quinto-Su, P. A., Hellman, A. N. & Venugopalan, V. Pulsed laser microbeam-induced cell lysis: time-resolved imaging and analysis of hydrodynamic effects. *Biophysical journal* **91**, 317–329 (2006).

[25] Hejnowicz, Z. & Kuczyńska, E. U. Occurrence of circular vessels above axillary buds in stems of woody plants. *Acta Societatis Botanicorum Poloniae* **56**, 415–419 (1987).

[26] West, J. L. & Cameron, I. D. Using the medical image processing package, imagej, for astronomy. *arXiv preprint astro-ph/0611686* (2006).

[27] Gilpin, W., Prakash, V. N. & Prakash, M. Vortex arrays and ciliary tangles underlie the feeding-swimming trade-off in starfish larvae. *Nature Physics* (2016). URL `http://dx.doi.org/10.1038/nphys3981`.

[28] Faubel, R., Westendorf, C., Bodenschatz, E. & Eichele, G. Cilia-based flow network in the brain ventricles. *Science* **353**, 176–178 (2016).

[29] Attanasi, A. *et al.* Collective Behaviour without Collective Order in Wild Swarms of Midges. *PLoS Comput Biol* **10**, e1003697 (2014). URL `http://dx.doi.org/10.1371%2Fjournal.pcbi.1003697`.

[30] Tunstrøm, K. *et al.* Collective states, multistability and transitional behavior in schooling fish. *PLoS Comput Biol* **9**, e1002915 (2013).

Journal of Experimental Biology • Advance article

[31] Batteen, M. L. & Han, Y.-J. On the computational noise of finite-difference schemes used in ocean models. *Tellus* **33**, 387–396 (1981).

[32] Foucaut, J.-M. & Stanislas, M. Some considerations on the accuracy and frequency response of some derivative filters applied to particle image velocimetry vector fields. *Measurement Science and Technology* **13**, 1058 (2002).

[33] Guasto, J. S., Johnson, K. A. & Gollub, J. P. Oscillatory flows induced by microorganisms swimming in two dimensions. *Physical review letters* **105**, 168102 (2010).

[34] Drescher, K., Goldstein, R. E., Michel, N., Polin, M. & Tuval, I. Direct measurement of the flow field around swimming microorganisms. *Physical Review Letters* **105**, 168101 (2010).

[35] Colin, S. P., Costello, J. H., Hansson, L. J., Titelman, J. & Dabiri, J. O. Stealth predation and the predatory success of the invasive ctenophore mnemiopsis leidyi. *Proceedings of the National Academy of Sciences* **107**, 17223–17227 (2010).

[36] Kiørboe, T. & Visser, A. W. Predator and prey perception in copepods due to hydromechanical signals. *Marine Ecology Progress Series* **179**, 81–95 (1999).

[37] Kasten, J., Reininghaus, J., Hotz, I. & Hege, H.-C. Two-dimensional time-dependent vortex regions based on the acceleration magnitude. *IEEE Transactions on Visualization and Computer Graphics* **17**, 2080–2087 (2011).

[38] Van Gelder, A. Vortex core detection: back to basics. In *IS&T/SPIE Electronic Imaging*, 829413–829413 (International Society for Optics and Photonics, 2012).

[39] Newton, P. K. *The N-vortex problem: analytical techniques*, vol. 145 (Springer Science & Business Media, 2013).

Journal of Experimental Biology • Advance article

[40] Beron-Vera, F. J., Olascoaga, M. J., Brown, M. G., Koçak, H. & Rypina, I. I. Invariant-tori-like lagrangian coherent structures in geophysical flows. *Chaos: An Interdisciplinary Journal of Nonlinear Science* **20**, 017514 (2010).

[41] Shadden, S. C., Lekien, F. & Marsden, J. E. Definition and properties of lagrangian coherent structures from finite-time lyapunov exponents in two-dimensional aperiodic flows. *Physica D: Nonlinear Phenomena* **212**, 271–304 (2005).

[42] Haller, G. Lagrangian coherent structures. *Annual Review of Fluid Mechanics* **47**, 137–162 (2015).

[43] Peacock, T. & Dabiri, J. Introduction to focus issue: Lagrangian coherent structures. *Chaos: An Interdisciplinary Journal of Nonlinear Science* **20**, 017501 (2010).

[44] Taylor, Z. J., Gurka, R., Kopp, G. A. & Liberzon, A. Long-duration time-resolved piv to study unsteady aerodynamics. *IEEE Transactions on Instrumentation and Measurement* **59**, 3262–3269 (2010).

[45] Shadden, S. C., Dabiri, J. O. & Marsden, J. E. Lagrangian analysis of fluid transport in empirical vortex ring flows. *Physics of Fluids (1994-present)* **18**, 047105 (2006).

[46] Johnson, P. L. & Meneveau, C. Large-deviation joint statistics of the finite-time lyapunov spectrum in isotropic turbulence. *Physics of Fluids (1994-present)* **27**, 085110 (2015).

[47] Haller, G. A variational theory of hyperbolic lagrangian coherent structures. *Physica D: Nonlinear Phenomena* **240**, 574–598 (2011).

[48] Schlueter-Kuck, K. L. & Dabiri, J. O. Coherent structure coloring: identification of coherent structures from sparse data using graph theory. *arXiv preprint arXiv:1610.00197* (2016).

Journal of Experimental Biology • Advance article

Figures

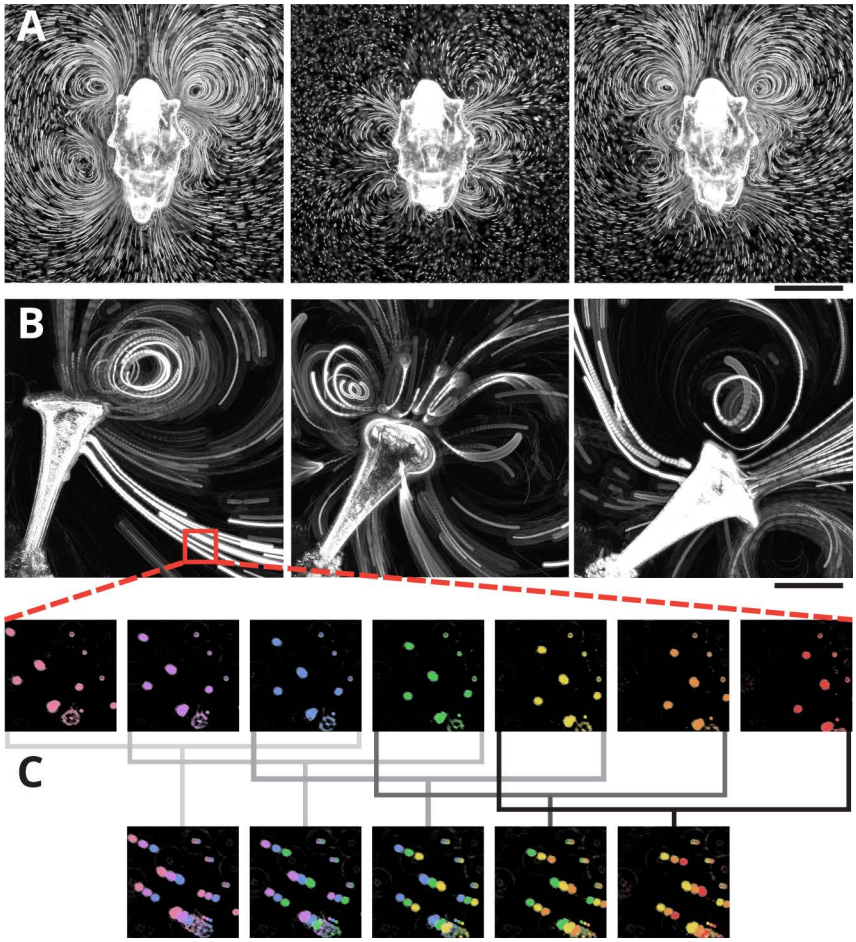

Figure 1 The Flowtrace algorithm. (**A.**) Three stills from a Flowtrace video of the feeding currents generated by the larva of the starfish *Patiria miniata*. (Supplementary Video 1 taken from Gilpin et al.;[27] $\tau = 3$ s, timepoints $= 0, 30, 90$ s, scale bar 500 μm). (**B.**) The gyration of the protozoan *Stentor sp.* as it filters water containing 6 μm beads (Supplementary Video 2; $\tau = 3$ s, timepoints $= 0, 6.5, 18$ s, scale bar 175 μm). (**C.**) A false-color detail from panel B illustrating the "sliding projection" used by Flowtrace to generate pathlines ($\tau = 3$ frames, scale bar 25 μm).

Journal of Experimental Biology • Advance article

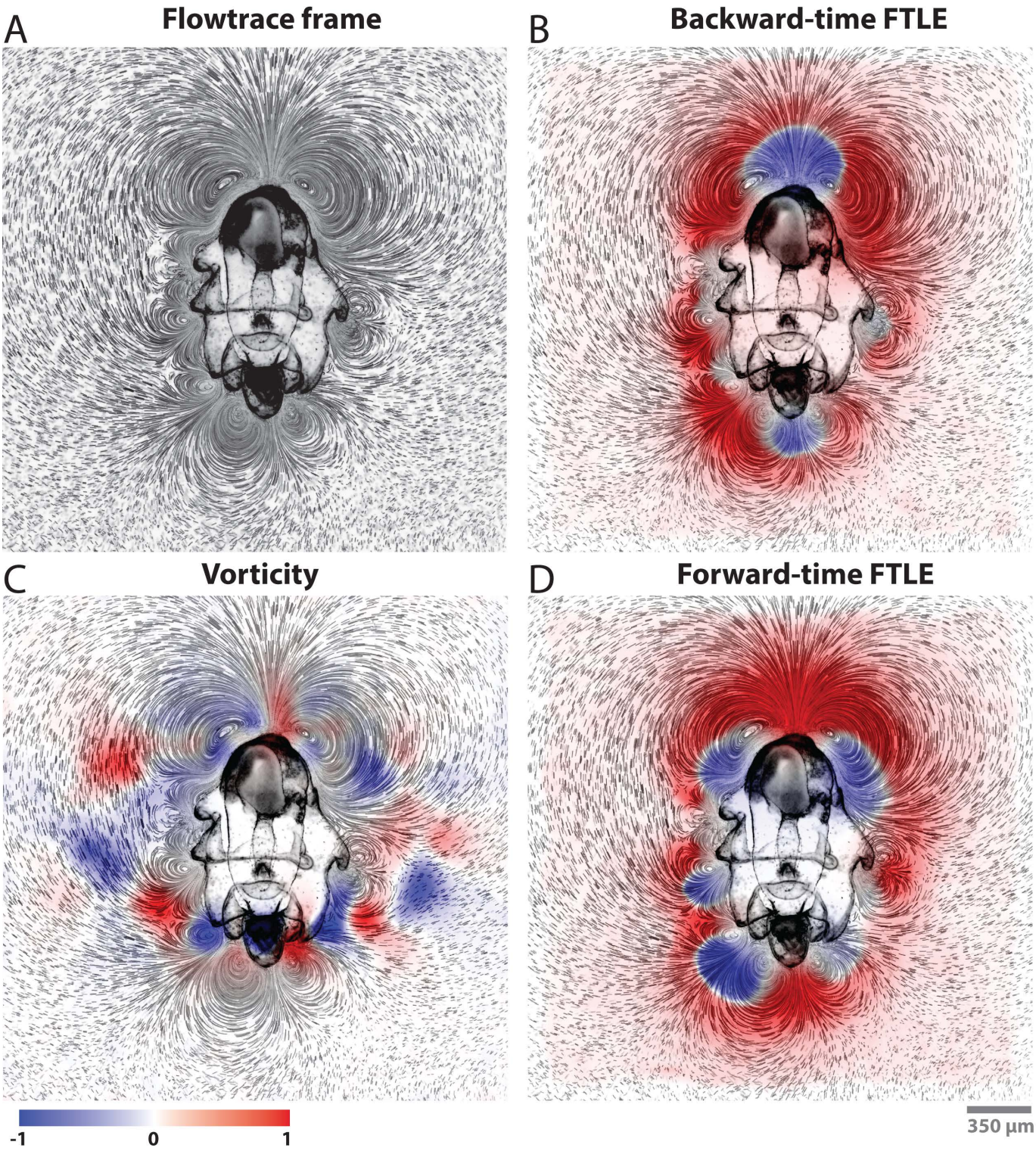

Figure 2 Comparison of Flowtrace with other methods for identifying coherent structures. All color plots have been rescaled so that the extremal absolute value of the scalar field being plotted corresponds to an intensity of 1, so that all color maps have the same range. Deep red regions in backward-time FTLE correspond to attracting coherent structures, whereas deep red regions in forward-time FTLE correspond to repelling structures. All colored scalar fields have been median-smoothed with a spatial kernel of a size smaller than the PIV mesh.

Journal of Experimental Biology • Advance article

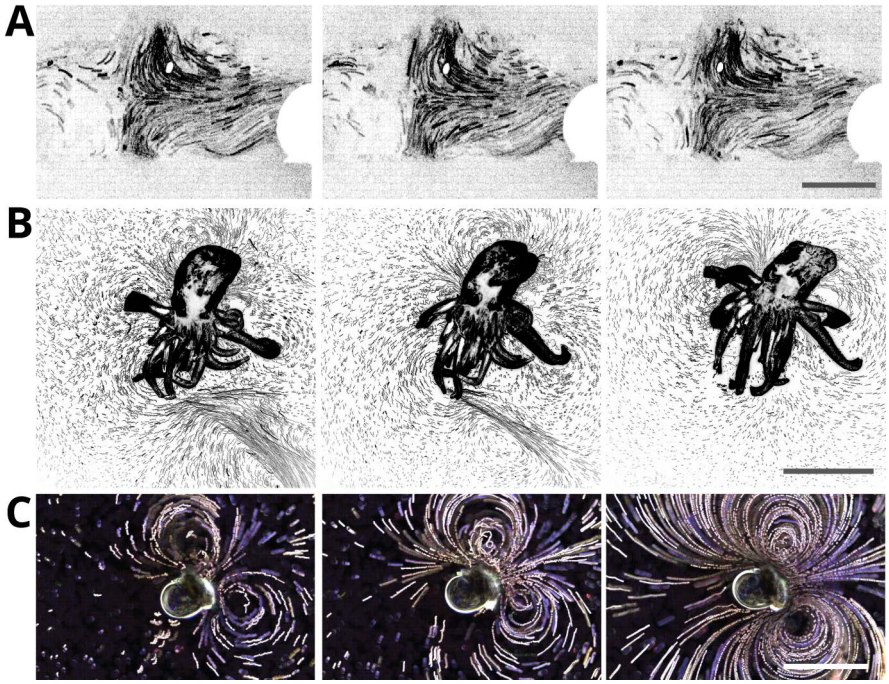

Figure 3 Application of Flowtrace to flow visualization problems. (**A.**) Transport of particles by the cerebrospinal fluid in a mouse's brain reveals the presence of a nearly-stationary hyperbolic stagnation point flow. Due to high particle density, the color of the original video has been inverted to ease visualization. (Supplementary Video S2 generated from data by Faubel et al;[28] $\tau = 0.67$ s, timepoints $= 0, 3, 6$ s, scale bar 50 μm) (**B.**) A sea anemone taking in a jet of water containing 6 μm beads. As above, the video has been inverted to ease visualization. (Supplementary Video S4; $\tau = 4$ min, timepoints $= 0, 5.4, 18$ min, scale bar 1 mm). (**C.**) A swimming moon snail larva, with 6 μm beads mixed into the water (Supplementary Video S5; $\tau = 2$ s, timepoints $= 0, 6, 20$ s, scale bar 350 μm).

Journal of Experimental Biology • Advance article

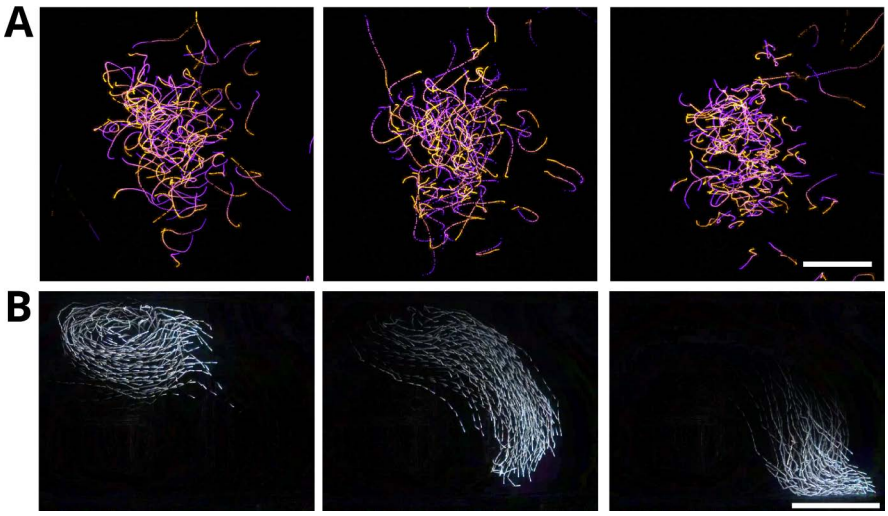

Figure 4 Flowtrace applied to collective animal motion. (**A.**) Three frames from a movie of a flock of midges, with pathlines temporally color-coded from blue to orange (Supplementary Video S6 generated from data by Attanasi et al;[29] $\tau = 333$ ms, timepoints $= 0, .66, 1.3$ s, scale bar 60 mm). (**B.**) A transition from "milling" to "swarming" behavior in a school of 70 minnows (Supplementary Video S7 generated from data by Tunstrøm et al.;[30] $\tau = 5.33$ s, timepoints $= 0, 9.1, 17.1$ s, scale bar 0.5 m).

Journal of Experimental Biology • Advance article